Buck Converter Current and Voltage Control by Exact Feedback Linearization with Integral Action

Juan S. Velez-Ramirez, Luis A. Rios-Noreña, Eduardo Giraldo

***Abstract*—The investigation about DC microgrids has become an important research axis due to its proved advantages in efficiency, sturdiness, reliability, and controllability. The first layer in every microgrid is composed of power electronic devices that must be designed and programmed to overcome the non-linearities and disturbances of a changing environment. In this paper, an Exact Feedback Linearization approach is proposed for control current or voltage in a Buck converter, designed to be part of a DC-microgrid. The controllers are tested in simulation using Matlab-Simulink®. Results are compared with classic PID controllers and evaluated under two different mathematical tools (Mean Square Error, Integral Time Absolute Error) in order to prove their effectiveness.**

***Index Terms*—Buck converter, DC Microgrid, Exact Feedback Linearization, linear control, non-linear control, Power electronics converters.**

I. Introduction

THE increasing demand of renewable energies sources operated in DC has lead to a growing interest in the DC generation, distribution, and transmission technologies [1], [2], photo-voltaic systems, battery energy storage, fuel cells, and electric vehicles are some examples. In the low voltage market, most loads can be operated in DC, such as internet servers, computers, led lighting, and a wide range of electronic devices. These changes in the conventional power grid lead to the concept of DC-microgrid [3], [4].

The literature refers enough definitions of a microgrid, depending on its design, features, and other aspects. In general, a microgrid is a cluster of distributed energy resources (generation, storage, and loads) that are integrated through power electronic converters, connected in parallel to share the load at a common bus, as depicted in Fig. 1 [2], [4]. One of the most important aspects of a microgrid operation is the capability to operate connected or disconnected of the main grid to avoid grid failures, as presented in [5] for distribution systems. Other remarkable aspects are the improvement of the energy quality of its local area network and the capability to sell or buy power depending on the local needs [6], [7], [8].

Several comparison studies conclude that the DC-microgrids are the best-suited structures for integration of renewable energy sources into the power grid, with flexibility, efficiency, and simplicity advantages [9], [10], [11].

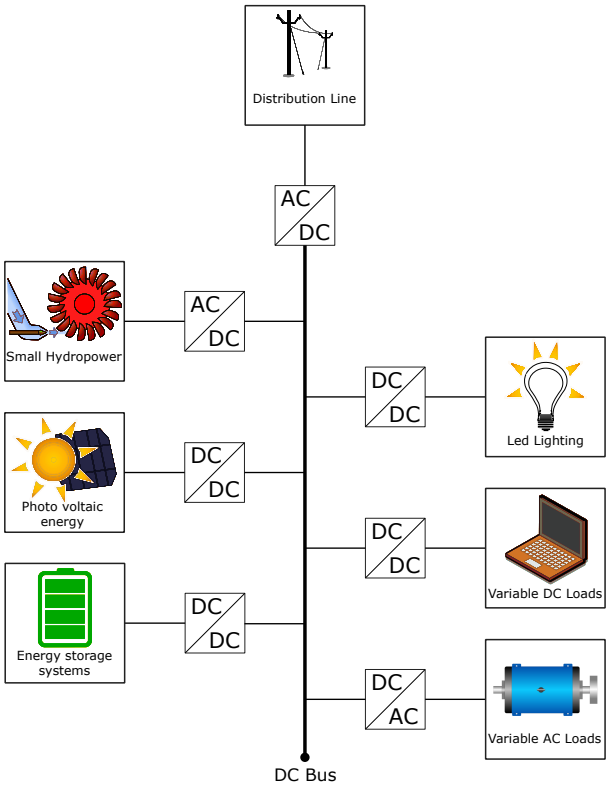

Fig. 1. Example of a DC microgrid with distributed energy resources.

The use of power electronic devices to convert the voltage levels and share the power between the distributed generators, the DC bus, and the local loads demand robust control techniques in the primary, secondary, and tertiary levels. As shown in Fig. 2, each step of the control design aims for specific objectives with the primary goal of stabilizing the standard microgrid variables: voltage, current, and the power-sharing between generation and demand nodes. These objectives must be achieved in both modes of operation, so the microgrid needs to ensure a stable and smooth transition during connection or disconnection of the main grid. With these operation conditions, the field level is subject to non-linear behaviors and a wide range of variations and disturbances that can affect the performance of the converter [11], [12], [13].

The constant search for more robust primary level controllers has become a relevant field of investigation in the state-of-the-art of DC distribution systems. The Buck converter has been widely studied in recent years due to its simplicity, reliability, and relatively low cost, which make it suitable to be part of every DC microgrid. Being a reducer-type converter, in exchange for the difference between input

Manuscript received July 6, 2020; revised November 17, 2020. This work is carried out under the funding of the Universidad Tecnológica de Pereira, Vicerrectoría de Investigación, Innovación y Extensión. Research project: 6-20-7 "Estimación Dinámica de estados en sistemas multivariables acoplados a gran escala".

J.S. Velez-Ramirez and L.A. Rios-Noreña are graduated students at the master on Electrical Engineering program, Universidad Tecnológica de Pereira, Pereira, Colombia.

e-mails: {jusever,luis.rios,egiraldos}@utp.edu.co.

E. Giraldo is a full professor at the Department of Electrical Engineering, Universidad Tecnológica de Pereira, Pereira, Colombia.

Research Group in Automatic Control.

e-mail: egiraldos@utp.edu.co.

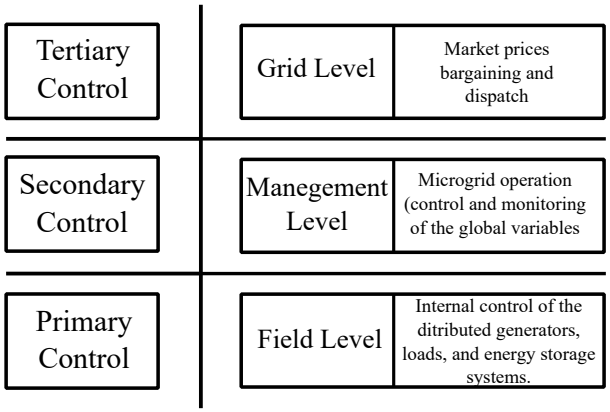

Fig. 2. General structure of the hierarchical control in microgrids.

and output voltages, the Buck converter can handle higher output currents than the input equivalent [14]. These facts make it suitable to be located in the load-side, controlling voltage, current or power of led-based illumination systems, internet servers, industrial automation arranges, and other DC loads.

As said above, a Buck converter integrated into a microgrid must have a robust controller with the capability to operate over contingencies and disturbances like changes in the input voltage or the load. This capability is required to improve the whole system performance. Multiple approaches to overcome this issue can be studied in the literature. Al-Rabadi et al. developed a model reduction technique using recurrent supervised neural networks that guarantee a simpler state feedback control [15]. A drawback of this research is that the designed controller is a well known linear technique, that doesn't have the sturdiness of non-lineal techniques. The same author explores a hierarchical intelligent hybrid PID-fuzzy logic controller, with proved sturdiness against disturbances [16], but the use of PID controllers, and the implementation of fuzzy logic, implies a well known behaviour of the system that is not available in all cases. In the same area, Swathy et al. proposed a fuzzy logic controller with output voltage regulation instead of changing circuit parameters [17]. However, even when the controller has a relatively good response, the absence of comparisons with the said linear methods and the lack of information about the inductor current could lead to misunderstandings. Boukerdja et al. present a robust H_∞ based control technique, with disturbance analysis and laboratory test [18], their investigation focuses on managing constant power loads and is highly supported in theoretical and experimental results. Its conclusion also leads to the complexity of the algorithm implementation and some issues in the laboratory set up. Finally, [19] and [20] are some examples of the developments in the sliding mode theory applied to power electronic devices, focusing in the voltage control and neglecting the importance of the current behavior in the model performance.

The Exact Feedback Linearization (EFL) is a non-linear control technique that searches for a linear transformation of non-linear systems. The objective is to construct a control signal that can eliminate nonlinearities' effects on the dynamic system's behavior. With a mathematical basis founded in the differential geometry, this theory could be applied in the power electronics field to improve a wide range of devices' performance [21], [22].

In this paper, an EFL technique with integral action is proposed for current and voltage control of a Buck converter. Proposed approach is compared with classic PID controllers for reference tracking and disturbance rejection. Obtained results show that the proposed approach outperform the classical methods in terms of Mean Square Error and Integral Time Absolute Error. This paper is organized as follows: In section II, this paper presents an approach to the Buck converter's design and modeling, as well as some aspects of current and voltage control techniques like the dynamic interpretation of the differential equation, the mathematical background, and the definition of the control laws. In sections III and IV are presented the experimental setup and results of the proposed approach compared to a linear control approach, with numerical analysis tools like the Mean Square Error (MSE) and the Integral Time Absolute Error (ITAE).

II. Theoretical framework

A. The Buck converter

As said above, this converter is suitable for DC-microgrid applications due to its behavior that amplifies the output current instead of the input voltage reduction. Therefore, larger loads in regulated low voltages like 12V or 24V are widely used in DC applications.

In Fig. 3, the classic electrical structure of a buck converter is shown, where E is the input voltage, μ is the boolean control signal that activates the electronic switch (usually a MOSFET or IGBT transistor), i is the inductor current, and v is the output voltage.

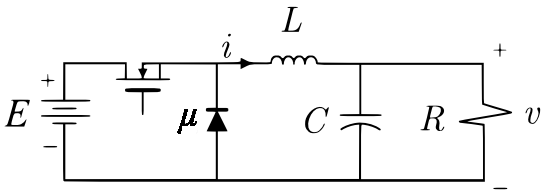

Fig. 3. General structure of a Buck converter

The constants of the model that define its operation characteristics are the inductance L in Henrys, the capacitance C in Farads, and the load resistance R in Ohms.

1) Design for microgrid applications: The design of a converter depends on its application. In this case, it must be part of a DC-microgrid with a structure, as shown in Fig. 1. The Buck converter could be connected to the DC bus, feeding the led lighting system or the variable DC-load node.

In terms of the design criteria, the most used switching strategy is the known pulse width modulation (PWM), in which the energy of the input voltage is managed by the time of the "On" state of the switch. In Fig. 4 is shown the behavior of the diode voltage during the PWM signal period (T).

This lets the introduction of the duty cycle variable (D), as a percentage of T, that can be expressed along with μ as presented in (1).

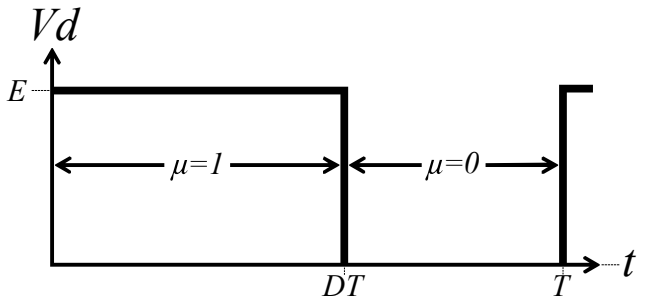

Fig. 4. Waveform of the diode voltage in period T of the PWM.

$$\mu = \begin{cases} 1; & 0 \leq t \leq DT \\ 0; & DT < t \leq T \end{cases} \tag{1}$$

Equation (1) can be simplified in terms of D giving (2).

$$\mu = \begin{cases} 1 & D \\ 0 & (1-D) \end{cases} \tag{2}$$

With this, it is possible to calculate the critical inductor and capacitor in terms of a continuous conduction mode of operation.

$$L_c = \frac{(1-D^*)R}{2f}; \quad C_c = \frac{1-D^*}{16L_c f^2} \tag{3}$$

where f is the switching frequency related to the switching period by expression (4), and D^* is the nominal value of the duty cycle in the equilibrium point. Being f defined as:

$$f = \frac{1}{T} \tag{4}$$

being T the time between two consecutive rising flanks.

With the above set of equations is possible to design a standard Buck converter in continuous conduction mode. It is important to note that E and R are taken theoretically as constants, but they are subject to disturbances that test the control's robustness in practice.

2) Dynamic Model: To obtain a proper dynamic model is a need to understand the input signal yield's behaviors in the system.

Let be the input $\mu = 1$. Then, Fig. 3 neglecting power losses, can be simplified as shown in Fig. 5.

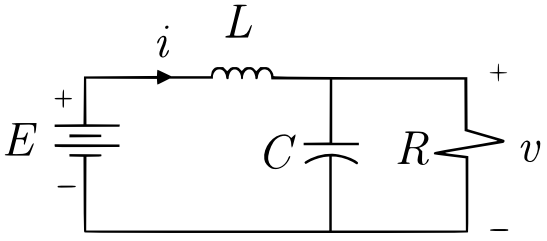

Fig. 5. Buck converter when $\mu = 1$, neglecting power losses

Defining the states of the new system (i,v), the differential equation that model its behavior in function of the time are (5).

$$L\frac{di}{dt} = E - v(t) \tag{5a}$$

$$C\frac{dv}{dt} = i(t) - \frac{1}{R}v(t) \tag{5b}$$

Now, let be $\mu = 0$. The new schematic of the converter could be simplified as shown in Fig. 6

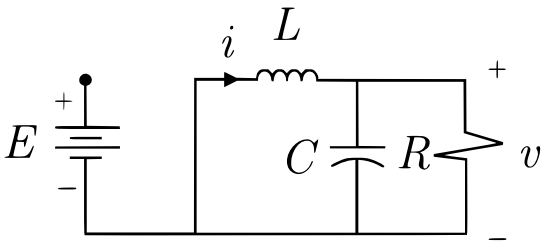

Fig. 6. Buck converter when $\mu = 0$, neglecting power losses

and the resulting differential equations are shown in (6), as follows:

$$L\frac{di}{dt} = -v(t) \tag{6a}$$

$$C\frac{dv}{dt} = i(t) - \frac{1}{R}v(t) \tag{6b}$$

The sets (5) and (6) depend exclusively on the state of the input signal μ. Multiplying (2) by both expressions respectively, the set (5) becomes (7).

$$L\frac{di}{dt} = \big(E - v(t)\big)D(t) \tag{7a}$$

$$C\frac{dv}{dt} = \left(i - \frac{1}{R}v(t)\right)D(t) \tag{7b}$$

The same procedure is performed with the set (6), resulting in (8).

$$L\frac{di}{dt} = -v(t)\big(1 - D(t)\big) \tag{8a}$$

$$c\frac{dv}{dt} = \left(i - \frac{1}{R}v\right)(1 - D) \tag{8b}$$

Finally, equations (7) and (8) are added in order to create an averaged model of converter, as presented in (9).

$$L\frac{di}{dt} = ED(t) - v(t) \tag{9a}$$

$$C\frac{dv}{dt} = i(t) - \frac{1}{R}v(t) \tag{9b}$$

The pack of equations (9) could be expressed in state space, as shown in (10).

$$\begin{bmatrix} \dot{x_1} \\ \dot{x_2} \end{bmatrix} = \begin{bmatrix} 0 & -\frac{E}{L} \\ \frac{1}{C} & -\frac{1}{RC} \end{bmatrix} \begin{bmatrix} x_1 \\ x_2 \end{bmatrix} + \begin{bmatrix} \frac{E}{L} \\ 0 \end{bmatrix} \Delta u \tag{10}$$

with (9) and (10) it is possible to introduce the different control strategies implemented below.

B. Behavior analysis

Calculation of the transfer function can throw essential facts about the dynamic response of the converter's state variables. By applying the Laplace transform to (9) and building the equivalent transfer functions of current (11) and voltage (12), it is possible to analyze some facts that guarantee the performance of the non-linear controllers [23].

$$I(s) = \frac{\left(\frac{E}{L}s + \frac{E}{LCR}\right) D(s)}{s^2 + \frac{1}{RC}s + \frac{1}{LC}} \tag{11}$$

$$V(s) = \frac{\frac{E}{LR}D(s)}{s^2 + \frac{1}{RC}s + \frac{1}{LC}} \tag{12}$$

One remarkable thing about the Buck converter is the zero location of both of the transfer functions. Unlike other kinds of converters like the Boost or the Buck-Boost, the Buck does not present zeros located on the positive side of the complex plane for both transfer functions. This means that it is a minimum-phase system, so the voltage and current have stable inner dynamics [23], [21]. Replacing the parameters of Table I in (11) and (12), described in section III, it is possible to get the poles and zeros values of both transfer functions.

Current transfer function is depicted in Fig. 7, and have a zero located in the negative side of the complex plane.

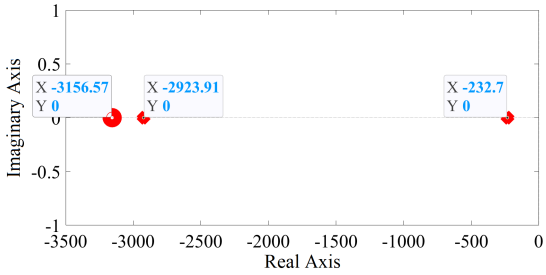

Fig. 7. Poles and zeros locations of the transfer function of current

Voltage transfer function has two poles and does not have zeros, as presented in Fig. 8.

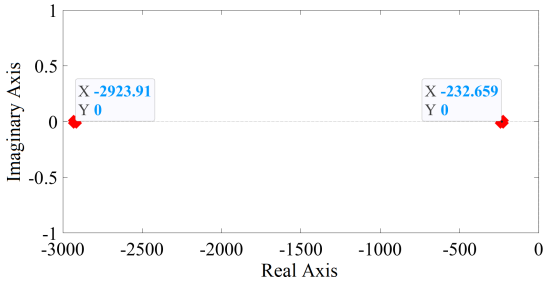

Fig. 8. Poles and zeros locations of the transfer function of voltage

This is a key to develop the EFL controllers since the order stability of the internal dynamic determines the designed control law's applicability. It can be concluded that both state variables: current, and voltage, have stable inner dynamics, so that an EFL technique could be proposed for each one [22].

C. Feedback linearization control

The generalized model of a nonlinear dynamic system is given by (13)

$$\dot{x} = f(x) + g(x)u(t) \tag{13}$$

A nonlinear state space model, where $x(t)$ is a vector that contains the state variables, and $f(x)$ and $g(x)$ are independent functions of x.

The set of equations of (9) can be transformed into state space model giving (14).

$$\dot{x_1} = \frac{V_{in}}{L}D(t) - \frac{1}{L}x_2(t) \tag{14a}$$

$$\dot{x_2} = \frac{1}{L}x_1(t) - \frac{1}{RC}x_2(t) \tag{14b}$$

where x_1 is the inductor current (i) and x_2 is the output voltage (v).

1) Current control: By defining the output of the system as $x_1(t)$, as is shown in (15).

$$y(t) = x_1(t) \tag{15}$$

The derivative of this equation is given by (16).

$$\dot{y}(t) = \dot{x_1} = \frac{E}{L}D(t) - \frac{1}{L}x_2(t) \tag{16}$$

In this case, for current control, the output of a second-order system appears in the first derivative, throwing a reduced-order control. This is not a problem since it was demonstrated that the current inner dynamics are stable. Thus, equation (16) can be compared to a corrective function Ψ as shown in (17).

$$\dot{x_1} = \Psi \tag{17a}$$

$$\frac{E}{L}D(t) - \frac{1}{L}x_2(t) = \Psi \tag{17b}$$

Defining $x_1(t)^*$ as the error (18), the following equation is obtained:

$$x_1(t)^* = x_1(t) - x_d(t) \tag{18}$$

where $x_d(t)$ is the reference. The function Ψ can be defined to guarantee a reference tracking, with a proportional gain K and an integral action that ensures the error correction, adjusting the value of the integral gain K_i. Resulting Ψ is (19).

$$\Psi = -Kx_1(t)^* + K_i e_i(t) \tag{19}$$

where $e_i(t)$, known as the integrative error, is defined as:

$$e_i(t) = \int_0^t x_1(\tau)^* d\tau \tag{20}$$

By applying derivatives at both sides of expression (20), the expression (21) is obtained.

$$\dot{e_i} = x_1(t)^* = x_1(t) - x_d(t) \tag{21}$$

A new closed-loop state space model can be built from the first order differential equations (17) and (21), as shown in (22).

$$\begin{bmatrix} \dot{x_1} \\ \dot{e_i} \end{bmatrix} = \begin{bmatrix} 0 & 0 \\ 1 & 0 \end{bmatrix} \begin{bmatrix} x_1 \\ e_i \end{bmatrix} + \begin{bmatrix} 1 \\ 0 \end{bmatrix} \Psi - \begin{bmatrix} 0 \\ 1 \end{bmatrix} x_d \quad (22)$$

and the control law that guarantee the reference tracking is given by (23), as follows:

$$D(t) = \left(-Kx_1(t)^* + K_i e_i(t) + \frac{1}{L} x_2(t) \right) \frac{L}{E} \quad (23)$$

Since the input voltage E is a non-controlled input instead of a constant, and for microgrids applications, must be a global variable available for all the primary level controllers, then the feedback of E ensures a fast response against changes in the main DC bus. This guarantees the operation of the node.

2) Voltage control: Unlike other standard converters, the Buck does not present unstable behaviors in the voltage loop side, this means that an EFL procedure can be developed. Lets define the voltage as the output of the system. In order to guarantee a linear transformation of the model, a new space must be defined, lets call this as the vector $z(t)$.

$$y(t) = x_2(t) = z_1(t) \quad (24)$$

The first derivative of (24) is given by (25).

$$\dot{z_1} = -\frac{1}{RC} x_2(t) + \frac{1}{C} x(t) = z_2(t) \quad (25)$$

Since the control signal D doesn't exist in the first derivative, the second derivative must be calculated. The resulting expression contains the control signal so it can be equalized to the corrective function Ψ as shown in (26).

$$\dot{z_2} = -\frac{1}{RC} x_1(t) + \left(\frac{1}{(RC)^2} - \frac{1}{LC} \right) x_2(t) + ... \\ ... \left(\frac{E}{LC} \right) D(t) = \Psi \quad (26)$$

where the corrective function V is designed for a complete order model. By adding the integral action, the expression (27) is obtained.

$$\Psi = -K_1 z_1(t) - K_2 z_2(t) + K_i e_i(t) \quad (27)$$

where the error is given by (28),

$$x_2(t)^* = x_2 - x_2 d \quad (28)$$

and the integrative error e_i given by (29)

$$e_i(t) = \int_0^t x_2(\tau)^* d\tau \quad (29)$$

The augmented state space model is presented in (30), as follows:

$$\begin{bmatrix} \dot{z_1}(t) \\ \dot{z_2}(t) \\ \dot{e_i}(t) \end{bmatrix} = \begin{bmatrix} 0 & 1 & 0 \\ 0 & 0 & 0 \\ 1 & 0 & 0 \end{bmatrix} \begin{bmatrix} z_1(t) \\ z_2(t) \\ e_i(t) \end{bmatrix} + \begin{bmatrix} 0 \\ 1 \\ 0 \end{bmatrix} \Psi - \begin{bmatrix} 0 \\ 0 \\ 1 \end{bmatrix} x_2 d \quad (30)$$

Clearing $D(t)$ from expression (26) is given the model's control law (31).

$$D(t) = \Big[-K_1 z_1(t) - K_2 z_2(t) + K_i e_i(t) + ... \\ ... \frac{1}{RC^2} x_1(t) + \left(\frac{1}{LC} - \frac{1}{(RC)^2} \right) x_2(t) \Big] \frac{LC}{E} \quad (31)$$

where $z_1 = x_2^*$ is defined in function of the error, and z_2 is defined by the expression (25).

As explained in section II-C2, feedback of the input voltage E might ensure a fast response against changes in the DC bus. In voltage control (31) is dependant of the load resistance R. In a variable load node, R could change abruptly, leading to instabilities. In the buck converter case, this problem can be solved by doing a digital calculation of the resistances value, from the known values of i and v. With this feedback, the control law is strong enough to overcome several disturbances at the load side.

III. Experimental Setup

A. Model constants

The Table I shows the model parameters, taking into account the critical inductor and capacitor given by (3).

TABLE I
PARAMETERS FOR CALCULATION AND SIMULATION DEVELOPMENT

NAME	SYMBOL	VALUE
Input voltage	E	$220v$
Switching frequency	f	$80kHz$
Capacitance	C	$220\mu F$
Inductance	L	$6.7mH$
Resistance	R	1.44Ω
Equilibrium Duty Cycle	D^*	11%

B. Simulation Settings

Simulations are made in Matlab-Simulink® with a duration of $230ms$. All controllers begin with the reference value in 0 and have a reference change at $t = 5ms$. For current, the new reference is set to $16.67A$, and for voltage, the reference is set to $24V$. In order to test the controllers' robustness, two different disturbances are programmed. The first one at $t = 110ms$, an input voltage loss of 30%. The second one, at $t = 150ms$, is a parallel connection of a resistive load equal to R's nominal value, simulating a sudden load increase.

To compare the performance of the EFL controllers, PID current and voltage controllers are tested with the simulation parameters. The gains of this method are adjusted with the *PID tune* environment of Simulink®. The constants of the non-linear controllers K and K_i, for current control, and K_1, K_2 and K_i, for voltage control, are adjusted experimentally. In order to establish the performance of each control technique, MSE and ITAE are applied to each simulation.

IV. Results and discussion

A. Current control

In Fig. 9 is depicted the response of PID (a) current controller, and EFL (b) current controller whose control law is defined by the expression (23). Note that both methods fulfill the objective, reaching the reference and overcoming the disturbances.

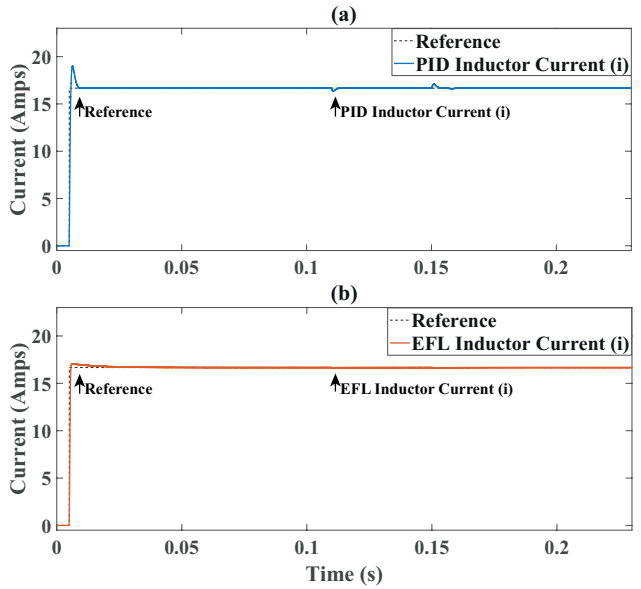

Fig. 9. Current controllers performance: (a) PID, (b) EFL.

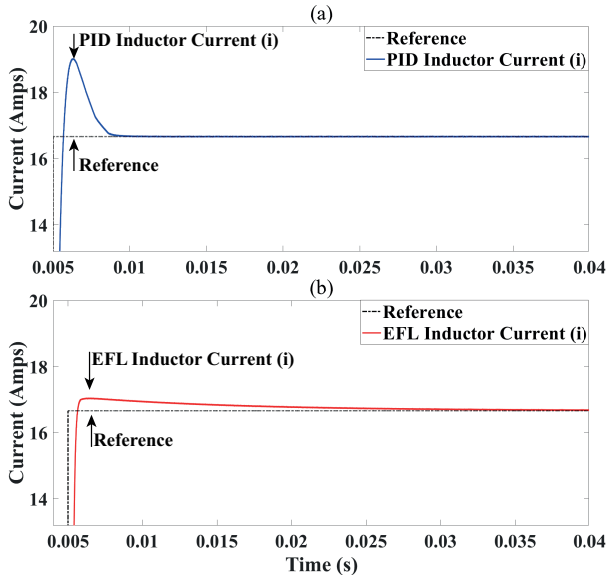

Fig. 10. Transient state behaviour: (a) PID current controller, (b) EFL current controller.

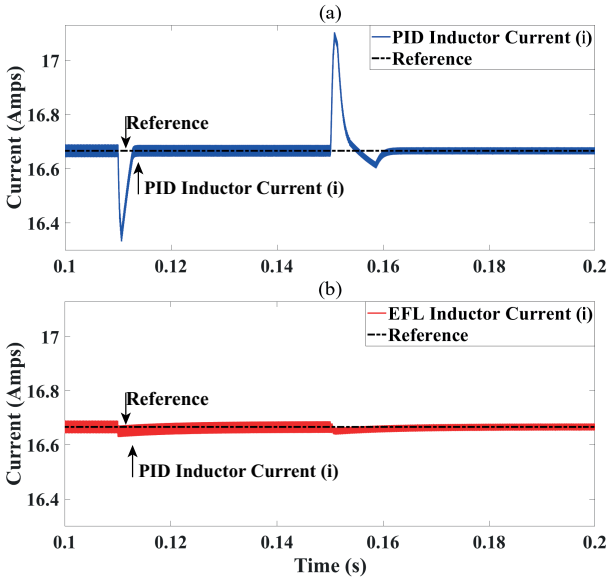

Fig. 11. Disturbance response behaviour: (a) PID current controller, (b) EFL current controller

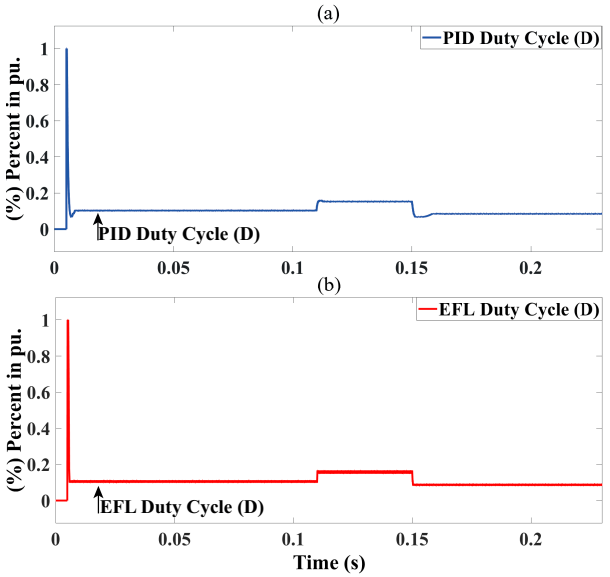

Fig. 12. Duty cycle response comparison: (a) PID current controller, (b) EFL current controller.

Due to the speed of both responses, a detailed analysis is presented. In Fig. 10 is shown the transitory response to the reference change at $t = 5ms$. There is a clear difference between both graphs. Fig. 10 (a), depicts a maximum overshoot of $2.3649A$ and a settling time less than $5ms$, instead Fig. 10 (b), depicts a maximum overshoot of $0.3963A$ and a settling time of $20ms$. It can be concluded that the EFL, although it is slower than the PID, has a better transient response.

In Fig. 11 is shown an approach to the disturbances between $t = 100ms$ and $t = 200ms$. Note that PID (a), has a current loss of $0.3347A$ at $t = 110ms$ due to the first disturbance. The same graph depicts a current increment of $0.4371A$ at $t = 150ms$ due to the load connection. EFL (b) does not present representative changes against any of the disturbances, showing more sturdiness than the PID control.

Additional information can be obtained by observing the other variables of interest that operate in the system. In Fig. 12 is shown the performance of the control signal, the duty cycle (D), through all the simulation. It can be seen that PID response (a), and EFL response (b), have a similar behaviour, with a slightly difference at the disturbances response, at $t = 5ms, 110ms, 150ms$. It is worth noting that the PID is slower but has less oscillations, meanwhile the EFL is faster, and virtually avoids the overshoots caused by the disturbances.

The output voltage response (v) presented in Fig. 13 shows the voltage behaviour through all the simulation, showing a sudden voltage loss at $t = 150ms$ due to the second load connection, equivalent to a half o the nominal output voltage $v = 12V$.

To clarify the results, Table II compare the MSE and ITAE measures of both controllers, where the higher performance of the current EFL controller is validated.

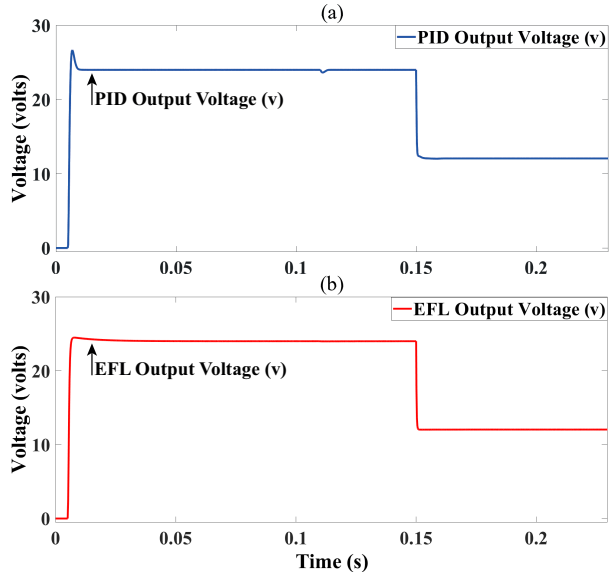

Fig. 13. Voltage response comparison: (a) PID current controller, (b) EFL current controller

TABLE II
COMPARISON OF CURRENT CONTROLLERS PERFORMANCE

CONTROL METHOD	MSE	ITAE
PID	$2.6482e+05$	$2.1765e+03$
EFL	$2.3316e+05$	$1.5045e+03$

B. Voltage control

In Fig. 14 is depicted the response of PID (a), and EFL (b) whose control law is defined by expression (31).

The transient response is clearer presented in Fig. 15, where PID (a), have a maximum overshoot of $1.7545V$, and a settling time less than $15ms$. In contrast, EFL (b), have a maximum overshoot of $2.0498V$, and a settling time less than $26ms$. In this case, PID control shows a better transient response.

Disturbances response is depicted in Fig. 16. The input voltage loss at $t = 110ms$, in PID graph (a), induce a sudden oscillation with a negative peak of $1.2738V$. Note that this

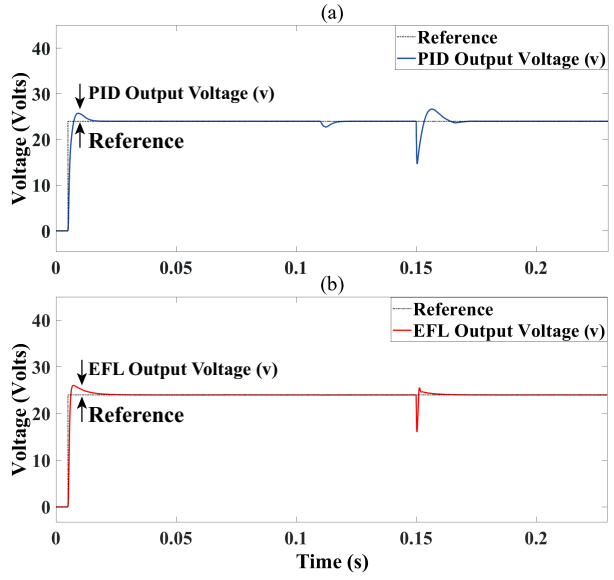

Fig. 14. Voltage controllers performance: (a) PID, (b) EFL.

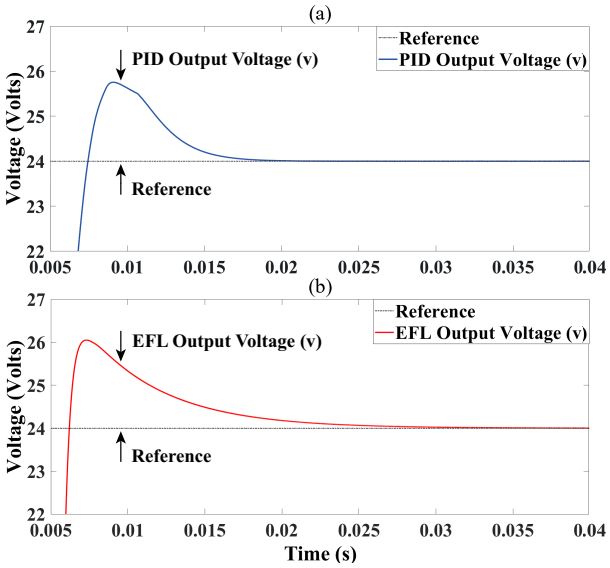

Fig. 15. Disturbance response behaviour: (a) PID voltage controller, (b) EFL voltage controller

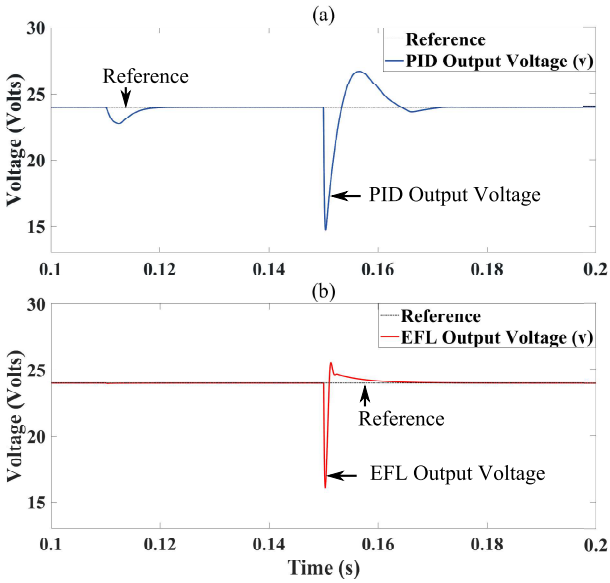

Fig. 16. Disturbance response comparison: (a) PID voltage controller, (b) EFL voltage controller.

disturbance is virtually ignored by the EFL (b). It can be seen that the extra load connection at $t = 150ms$ trigger a highly oscillatory response in both methods. On the other hand, the PID reaches a maximum deviation of $9.3431V$. However, the EFL reaches a maximum deviation of $7.9628V$. Therefore, the EFL with input voltage (E), and load (R) feedback, demonstrate better sturdiness than the PID control.

The control signal comparison is presented in Fig. 17.

In this case EFL, of Fig. 17 (b), have a more aggressive response compared with the PID, of Fig. 17 (a). In order of overcome the disturbances at $t = 150ms$, the EFL duty cycle shows a higher oscillatory peak. This should be the study object of future research.

The behaviour of the current with the voltage controllers is presented in Fig. 18. It can be seen that both models ensure acceptable stability even in front of major disturbances. At $t = 150ms$ the second load is connected in parallel, demanding an increase on the output current, equivalent to

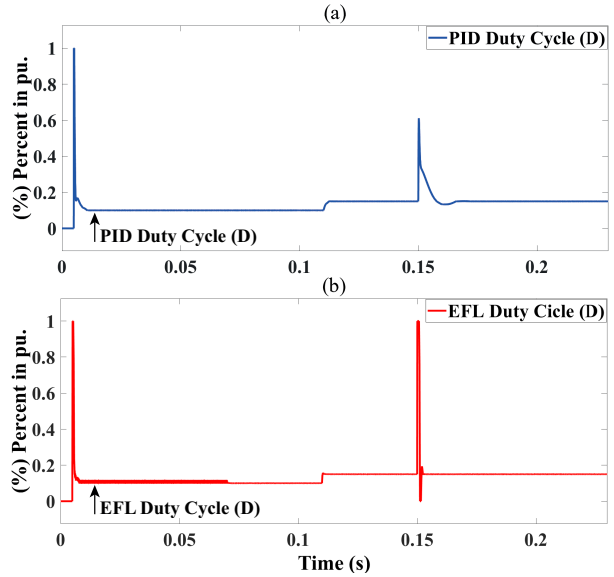

Fig. 17. Duty cycle response comparison: (a) PID voltage controller, (b) EFL voltage controller.

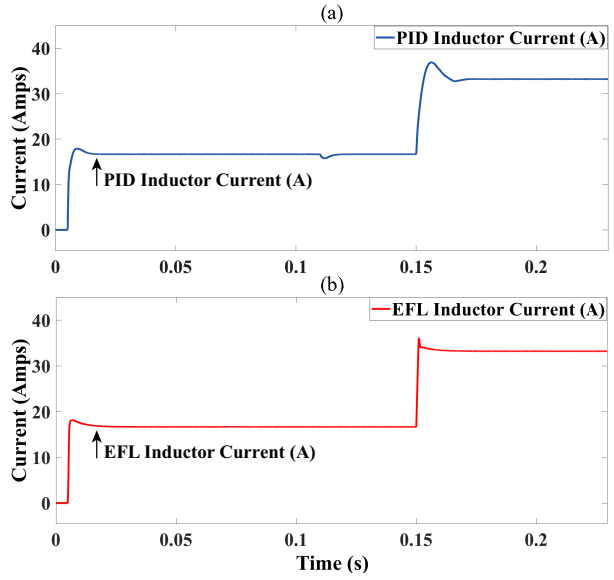

Fig. 18. Inductor current response comparison: (a) PID voltage controller, (b) EFL voltage controller.

the nominal value of the inductor current $i = 16.66A$.

To clarify the results, Table III compare the MSE and ITAE measures resulting from the experimental setup for both controllers. In this case, the higher performance of the voltage EFL controller against the voltage PID controller, is proved by a narrow margin.

TABLE III
COMPARISON OF VOLTAGE CONTROLLERS PERFORMANCE

CONTROL METHOD	MSE	ITAE
PID	$2.0264e+06$	$2.8987e+04$
EFL	$1.3401e+06$	$8.8262e+03$

V. CONCLUSION

Two different EFL controllers for current and voltage regulation of a Buck converter are designed, tested, and compared to a well-known PID control method. Despite being based in a reduced order model, the current controller shows better performance and sturdiness than the usual PID. Another feature of this controller is its simplicity and relative easy adjustment. The non-linear voltage controller has shown a slight advantage in comparison with the PID, but, just like the PID, the difficulty to tune adequately the controller parameters adds complexity to the tuning. For future work, a voltage controller with self-tuning parameters will be proposed, where an indirect voltage controller, adjusting the references current value of the current EFL method's in function of a desired output voltage, will be included.

REFERENCES

[1] P. Brian, "DC, Come Home: DC Microgrids and the Birth of the "Enernet"," *IEEE Power and Energy Magazine*, vol. 10, no. 6, pp. 60–69, 2012.

[2] J. S. Velez, S. Ospina, and E. Giraldo, "Passivity-based control for a buck-boost converter applied in small wind generation interconnected to DC microgrid," *4th IEEE Colombian Conference on Automatic Control: Automatic Control as Key Support of Industrial Productivity, CCAC 2019 - Proceedings*, 2019.

[3] A. T. Elsayed, A. A. Mohamed, and O. A. Mohammed, "DC microgrids and distribution systems: An overview," 2015.

[4] B. Hernandez, E. Giraldo, S. Ospina, and A. Garces, "Master-slave operation of DC microgrids: An adaptive control approach with estimation," in *4th IEEE Colombian Conference on Automatic Control: Automatic Control as Key Support of Industrial Productivity, CCAC 2019 - Proceedings*, 2019.

[5] J. A. Villegas-Florez, B. S. Hernandez-Osorio, and E. Giraldo, "Multi-objective optimal control of resources applied to an electric power distribution system," *Engineering Letters*, vol. 28, no. 3, pp. 756–761, 2020.

[6] R. H. Lassater, "MicroGrids," in *2002 IEEE Power Engineering Society Winter Meeting. Conference Proceedings (Cat. No.02CH37309)*. New York, NY, USA, USA: IEEE, 2002, pp. 305–308. [Online]. Available: https://ieeexplore.ieee.org/abstract/document/985003

[7] L. Fusheng, L. Ruisheng, and Z. Fengquan, *Microgrid Technology and Engineering Application*. Joe Hayton, 2016. [Online]. Available: http://www.sciencedirect.com/science/article/pii/B9780128035986000115

[8] S. Parhizi, H. Lotfi, A. Khodaei, and S. Bahramirad, "State of the art in research on microgrids: A review," *IEEE Access*, vol. 3, pp. 890–925, 2015.

[9] H. Lotfi and A. Khodaei, "AC versus DC microgrid planning," *IEEE Transactions on Smart Grid*, vol. 8, no. 1, pp. 296–304, 2017.

[10] J. J. Justo, F. Mwasilu, J. Lee, and J. W. Jung, "AC-microgrids versus DC-microgrids with distributed energy resources: A review," *Renewable and Sustainable Energy Reviews*, vol. 24, pp. 387–405, 2013. [Online]. Available: http://dx.doi.org/10.1016/j.rser.2013.03.067

[11] E. Planas, J. Andreu, J. I. Gárate, I. Martínez De Alegría, and E. Ibarra, "AC and DC technology in microgrids: A review," 2015.

[12] A. Mehrizi-Sani, "Distributed Control Techniques in Microgrids," *Microgrid: Advanced Control Methods and Renewable Energy System Integration*, pp. 43–62, 2016.

[13] H. Yang, Q. Li, and W. Chen, "Microgrid communication system and its application in hierarchical control," *Smart Power Distribution Systems: Control, Communication, and Optimization*, pp. 179–204, 2018.

[14] M. H. Rashid, "Electronica de Potencia Muhammad Rashid 3ª.pdf," p. 904, 2004.

[15] A. N. Al-rabadi and O. M. K. Alsmadi, "Model Reduction-Based Control of the Buck Converter Using Linear Matrix Inequality and Neural Networks," *Lecture Notes in Engineering and Computer Science*, vol. 2175, no. 1, pp. 1367–1377, 2009.

[16] A. N. Al-Rabadi, M. A. Barghash, and O. M. Abuzeid, "Intelligent regulation using genetic algorithm-based tuning for the fuzzy control of the power electronic switching-mode Buck converter," *IAENG International Journal of Computer Science*, vol. 38, no. 4, pp. 320–342, 2011.

[17] K. Swathy, S. Jantre, Y. Jadhav, S. M. Labde, and P. Kadam, "Design and Hardware Implementation of Closed Loop Buck Converter Using Fuzzy Logic Controller," *Proceedings of the 2nd International Conference on Electronics, Communication and Aerospace Technology, ICECA 2018*, no. Iceca, pp. 175–180, 2018.

[18] M. Boukerdja, A. Chouder, L. Hassaine, B. O. Bouamama, W. Issa, and K. Louassaa, "H∞ based control of a DC/DC buck converter feeding a constant power load in uncertain DC microgrid system," *ISA Transactions*, 2020.

[19] B. B. Naik and A. J. Mehta, "Sliding mode controller with modified sliding function for DC-DC Buck Converter," *ISA Transactions*, 2017.

[20] G. Ma, B. Wang, D. Xu, and L. Zhang, "Switching control strategy based on non-singular terminal sliding mode for buck converter in auxiliary energy source," *Energy Procedia*, vol. 145, pp. 139–144, 2018. [Online]. Available: https://doi.org/10.1016/j.egypro.2018.04.023

[21] H. Sira-Ramírez, R. Márquez, F. Rivas-Echeverría, and O. Llanes-Santiago, *Control de Sistemas No Lineales*. Prentice Hall, 2004.

[22] Q. Lu, Y. Sun, and S. Mei, *Nonlinear Control Systems and Power System Dynamics*. Kluwer Academic Publishers, 2001.

[23] S. Ospina-Hurtado, *Análisis de controladores no lineales para convertidor DC-DC tipo BUCK-BOOST aplicado a un generador eólico*. Master Thesis, Universidad Tecnológica de pereira, 2019.